

Optimizing Laser-Induced Graphene Production

Lars KOTTHOFF^{a,1}, Sourin DEY^a, Jake HEIL^a, Vivek JAIN^a, Todd MULLER^a,
Alexander TYRRELL^a, Hud WAHAB^a, and Patrick JOHNSON^a

^a*Center for Artificially Intelligent Manufacturing, University of Wyoming, 1000 E
University Ave, Laramie, WY 82071, USA*

Abstract. A lot of technological advances depend on next-generation materials, such as graphene, which enables better electronics, to name but one example. Manufacturing such materials is often difficult, in particular, producing graphene at scale is an open problem. We apply state-of-the-art machine learning to optimize the production of laser-induced graphene, an established manufacturing method that has shown great promise. We demonstrate improvements over previous results in terms of the quality of the produced graphene from a variety of different precursor materials. We use Bayesian model-based optimization to quickly improve outcomes based on little initial data and show the robustness of our approach to different experimental conditions, tackling a small-data problem in contrast to the more common big-data applications of machine learning. We analyze the learned surrogate models with respect to the quality of their predictions and learned relationships that may be of interest to domain experts and improve our understanding of the processes governing laser-induced graphene production.

Keywords. Graphene, Bayesian optimization, applications of AI

1. Introduction

Graphene is a two-dimensional honeycomb layer of carbon atoms with extraordinary properties, for example relative strength higher than any other material, high conductivity of electricity and heat, and near transparency. It has many promising applications, such as next-generation semiconductors, flexible electronics, and smart windows, to name but a few examples [1]. There already are commercially available products made from or with graphene, and the size of the global market is currently about US-\$100 million, with significant growth forecast. However, the reliable and large-scale production of graphene is a difficult problem that researchers have been tackling over the past decades.

One method of producing graphene is to convert natural sources of carbon, e.g. graphite, coal, and biochar, into graphene oxide, which is soluble in water. Such solutions can be used as graphene oxide inks and be printed directly onto substrates as thin films, similar to how ink-jet printers deposit ink on paper. Irradiating this precursor material with a laser heats and anneals the graphene oxide selectively to reduce the oxygen, ultimately converting it into pure graphene. Similar results can be achieved by ir-

¹Corresponding Author: Lars Kotthoff, larsko@uwoyo.edu

radiating commercial polymer films, eliminating the need to manufacture and deposit graphene oxide, which is time-consuming in itself, or indeed any carbon precursor material [2]. The reduction of such precursor materials into graphene allows for the rapid and chemical-free manufacturing of advanced devices such as electronic sensors [3], fuel cells [4], supercapacitors [5,6], and solar cells [7]. The interested reader is referred to a recent survey on laser-induced graphene for more information [8]. This process is also referred to as laser-reduced graphene in the literature [9].

One of the advantages of the targeted irradiation of the precursor material is that it allows to easily create patterns in solid substrates without pre-patterned masks in only a few minutes. While graphene is electrically conductive, graphene oxide and polymers are not – patterns of graphene in an insulating material can form electric circuits. The laser irradiation process enables the scalable and cost-efficient fabrication of miniaturized electronic devices in a single process, rather than manufacturing the graphene separately and then patterning it onto a carrier material. This process also ensures that only the amount of material that is actually needed is produced, similar to other advanced manufacturing processes like 3D printing.

The challenge in irradiating the precursor material is determining the best laser parameters and reaction environment. First-principles knowledge does not allow to derive the optimal conditions and the effectiveness of different irradiation conditions varies across different precursor materials. A recent study emphasizes the effect the irradiation parameters have on the quality of the produced graphene and the need to optimize these parameters to achieve good results in practice [10]. Even with just a few parameters, for example the power applied to the laser and the duration for irradiating a particular spot, the space of possibilities is too large to explore exhaustively. There are complex interactions between parameters, and evaluating a particular parameter configuration involves running an experiment that requires a skilled operator and precursor material of sufficient quality. Exploring the space of experimental parameters efficiently is crucial to the success of laser-induced graphene in practice.

We present the application of state-of-the-art model-based optimization (MBO) techniques to the automated production of laser-induced graphene, improving the quality of the produced graphene significantly compared to results achieved in the literature. These improvements translate directly into better advanced materials that will enable the next generation of advanced electronics and their cost-efficient production. Our MBO system is deployed and used by domain scientists, with first results published in in the domain literature [11]. In this paper, we present a more in-depth analysis of the previous results and new results on the patterning of lines. While there have been applications of model-based optimization in other areas of materials science, e.g. [12,13], we present the first application to laser-induced graphene, to the best of our knowledge.

2. Methodology and Experimental Setup

The graphene oxide samples investigated in this paper were prepared from graphite using the improved Hummers' method, which avoids the generation of hazardous gases such as NO and NO_2 from nitrate that is used in the conventional Hummers' method [14]. Powdered samples, ground and sieved to $20\ \mu\text{m}$, were mixed in concentrated H_2SO_4 and H_3PO_4 and placed in an ice bath. $KMnO_4$ was added at a mixture temperature of $35\ ^\circ\text{C}$

and increased to 98 °C before termination with ultrapure water (Millipore) and H_2O_2 . The filtrate was then washed with HCl and repeatedly with water until a pH-level of about 6.5 was obtained. The GO inks were produced using 25 mg of the freeze-dried GO powder, diluted in 100 mL deionized water and ultrasonicated with a cooling system. After the sample was centrifuged, the remaining supernatant was repeatedly diluted and ultrasonicated until a 200 mL dilution was obtained. The GO inks were spray-coated onto a 1 cm×1 cm quartz or polyimide substrate (Kapton HN 125 μm, Dupont) in multiple passes until a thickness of 1 μm was achieved, verified with an optical profilometer.

Laser-induced graphene (LIG) spots were patterned by reducing GO films deposited on quartz and polyimide, and by carbonization of polyimides directly. We denote GO on quartz, GO on polyimide and polyimide as samples GOQ, GOPI and PI, respectively. The patterning setup is shown in Figure 1. The deposited GO films were placed in a sample chamber which allows patterning in air, argon, or nitrogen environments with pressures up to 1000 psi. LIG patterns were irradiated using a 532 nm diode-pumped solid-state continuous-wave laser. The laser beam was focused with a 50x microscope lens to a spot size of 20 μm on the sample surface. Irradiated beam spots were positioned sufficiently far apart from each other to ensure pristine precursor material for each experiment. The sample area is about 1 cm², allowing approximately 256, 25, and 25 patterns for samples GOQ, GOPI, and PI, respectively. Taking into account sample preparation and repeated measurements to account for experimental errors and ensure reproducibility, we set our experimental budget to 70 for all types of samples.

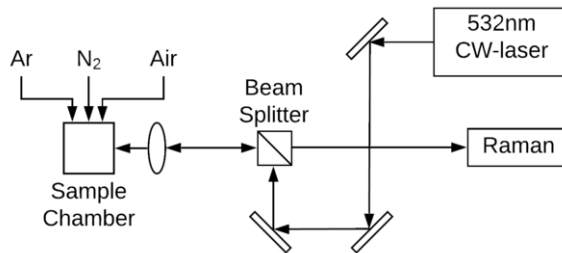


Figure 1. Experimental setup for patterning and measuring laser-induced graphene. The unlabeled rectangles represent mirrors to reflect the laser beam, the ellipse a lens to focus it.

Additionally, we patterned LIG lines on GOQ using the same experimental setup, but restricted to an argon environment with pressures up to 350 psi. The lines had a length of 2 mm spaced 1 mm apart, totaling 14 lines within the sample area of 1 cm².

Raman spectroscopy is a common technique for determining the quality of laser-induced graphene by observing how laser photons scatter after they interact with the vibrating molecules in the sample probe. The intensities of the characteristic D and G bands in the Raman spectra can be used to judge to what extent the precursor material has been reduced to graphene, i.e. the quality of the resulting material. The D and G bands result from the defects and in-plane vibrations of sp² carbon atoms, respectively. In particular, the degree of reduction of the precursor material to graphene, and thus the

conductivity of the irradiated area, can be quantified through the ratio of the intensities of the G and D bands – the larger this ratio, the more the precursor material has been reduced. Figure 2 shows an example.

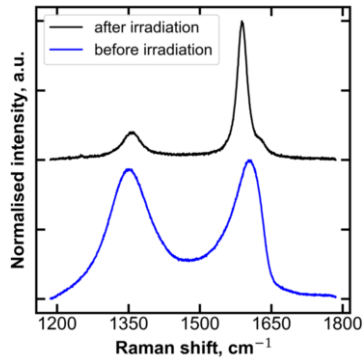


Figure 2. Raman spectra showing D (left peak) and G (right peak) bands of graphene oxide before (bottom) and after (top) laser irradiation. The ratio we optimize in this paper is calculated from the area under the peaks. The intensity is shown in arbitrary units (a.u.).

We filtered the backscattered laser beam through a long-pass filter after irradiation to perform Raman spectroscopy. Using the same laser source for patterning and spectroscopy, we are able to characterize the identical spot in-situ. The Raman data for each spot were averaged over 10 measurements with a collection time of 3 s at laser power < 10 mW for each measurement. The Raman spectra were post-processed with a linear background subtraction to 0 and normalization of the maximum peak to 1. The G- and D-bands were fitted using Lorentzian functions and the ratio of their intensities computed as the ratio of the areas under the fitted functions. The G/D ratios indicate the degree of reduction of GO to graphene. This measure can be used as a proxy for electric conductivity, which we cannot measure for an irradiated spot because of physical constraints.

For the LIG-patterned lines, we quantified the conductivity of the induced graphene by uniformly printing silver contacts (Voltera V-One, Ontario) at each end of each line and measuring the electrical resistance with a two-point probe. Results were averaged over nine individual measurements. We note that these measurements are only possible by removing the sample from the reaction chamber, i.e. after 14 lines have been patterned, as removing and replacing the sample after each line is too much human effort to be feasible in practice (in particular realigning the sample would be a very time-consuming task). This means that, different to the G/D ratio, the results of an experimental evaluation are only available after a complete batch has been evaluated.

2.1. Parameter Space

We consider the following four parameters of the experimental conditions that control the irradiation process for the spots.

- The power applied to the laser used to irradiate the sample. We consider a power range of 10 mW to 5550 mW, with a precision of 10 mW and a step size of 10 mW.

- The duration a particular spot was irradiated by the laser. We vary this parameter from 500 ms to 20000 ms, with a precision of 1 ms and a step size of 1 ms.
- The pressure in the reaction chamber. The values for this parameter range from 0 psi to 1000 psi, with a precision of 10 psi and a step size of 10 psi.
- The gas in the reaction chamber. Possible values for this parameter are argon, nitrogen, and air.

For the lines, we considered the following parameter space.

- We limited the power range to 10 mW to 1190 mW to avoid damage to the sample we observed for high powers in some cases [11]. The precision was 10 mW and the step size 10 mW.
- The patterning speed was varied between 0.267 mm s^{-1} to 1.905 mm s^{-1} . This is dictated by the physical limits of the motor moving the sample chamber. The step size and precision were 0.001 mm s^{-1} .
- The pressure in the reaction chamber. The values for this parameter range from 0 psi to 350 psi, with a precision of 10 psi and a step size of 10 psi.
- The gas in the reaction chamber was limited to argon, based on results from irradiating spots where argon performed better.

These parameters give rise to a large space of possible combinations that is infeasible to explore exhaustively. The cost of gathering data is high – running experiments is time-consuming and requires precursor materials to be available. In contrast to big-data approaches, we need techniques that work with small amounts of data, such as the MBO we apply here.

2.2. Model-Based Optimization

Bayesian model-based optimization techniques (MBO) are used in many areas of AI and beyond to automatically optimize outcomes across large parameter spaces. They usually proceed in an iterative fashion – choose the configuration to evaluate based on predictions of the surrogate model, and augment the surrogate model with the result of this evaluation for the next iteration. At the heart of these techniques are the surrogate models, which approximate and model the process whose parameters are to be tuned. This underlying process is expensive to evaluate, i.e. it is infeasible to exhaustively explore the parameter space and we are interested in keeping the number of evaluations as small as possible. The approximate surrogate model on the other hand is cheap to evaluate and allows for a targeted exploration of the parameter space, identifying promising configurations that available resources for evaluations of the underlying process should be directed towards.

Surrogate models are induced using machine learning, taking an increasing amount of ground-truth data into account between subsequent iterations. State-of-the-art MBO approaches often use Gaussian Processes or random forests to induce surrogate models, depending on the nature of the parameter space. MBO is a mature approach that has been used in many applications over decades. The interested reader is referred to the paper that formalized the approach [15] for more information.

There are many implementations of MBO; we use the mlrMBO package [16] to model the parameter space, build the surrogate models (with the mlr package [17]), and determine the most promising configuration for the next evaluation of the underlying process. In particular, we use the default random forest surrogate model for parameter

spaces that contain non-continuous parameters (the gas in the reaction chamber), and Gaussian Processes for the parameter space for the patterning of the lines that contains only continuous parameters, with expected improvement as our acquisition function in both cases. In each iteration of the optimization process, the next configuration or batch of configurations to evaluate is proposed by mlrMBO. Each configuration is set automatically by the experimental setup, which proceeds with running the experiment and evaluating its result for the irradiated spots. The evaluated parameter configuration and the resulting G to D ratio is added to the data used to train the surrogate model for the next iteration. For the resistance measured for lines of graphene, we propose batches of 14 parameter settings to evaluate using the “constant liar” strategy [18]; the surrogate model is retrained for the next MBO iteration after 14 such evaluations.

The initial surrogate model for the irradiated spots and G/D measurements was trained on 20 randomly-sampled parameter configurations. We then performed 50 iterations of our model-based optimization approach. For each of the three investigated materials GOQ, GOPI, and PI, we ran three experimental campaigns for a total of nine experimental campaigns and 630 patterned spots. This represents several weeks of experimental effort, in addition to the effort of preparing the samples. We ran three experimental campaigns for each material to assess the impact of different randomly-sampled initial data, as well as the effect of variations in the material itself.

The experiments patterning lines had a total experimental budget of nine samples for a total of 126 lines. One of the samples (14 parameter configurations) was used to evaluate configurations randomly sampled from the parameter space to train the initial surrogate model. The remaining eight samples were used to optimize the resistance of the patterned material. As patterning lines consumes considerably more precursor material than spots, the number of evaluations we were able to perform here is much smaller. We did not use any information from the patterning of spots to initialize the optimization of line patterning – it is not obvious how to transfer the best configurations.

The code, data, and some variations of our approach are available at <https://github.com/aim-uwyo/lig-model-opt> and as supplementary material for [11]. Our approach and code has since been used by other groups for similar purposes [19].

3. Results and Analysis

We first present the results for patterning spots of graphene and optimizing the G/D ratio in detail. Figure 3 shows the quality of the graphene produced for all of our nine experimental campaigns and Table 1 summarizes the results numerically. We note that performance improves as soon as we evaluate configurations that were determined to be promising by the model-based optimization approach compared to the initial random data. We achieve performance improvements for all three materials and on each of the experimental campaigns except one. Our approach is robust to differences in the initial data and irradiated materials. The performance improvements compared to random search are particularly large for graphene oxide on polyimide (GOPI, second graph). For the experiments on polyimide samples (PI, third graph) we achieve the smallest improvements over random parameter configurations and in one experimental campaign no improvement over the best configuration found in the initial random samples at all, owing to the very good results of the initial random search.

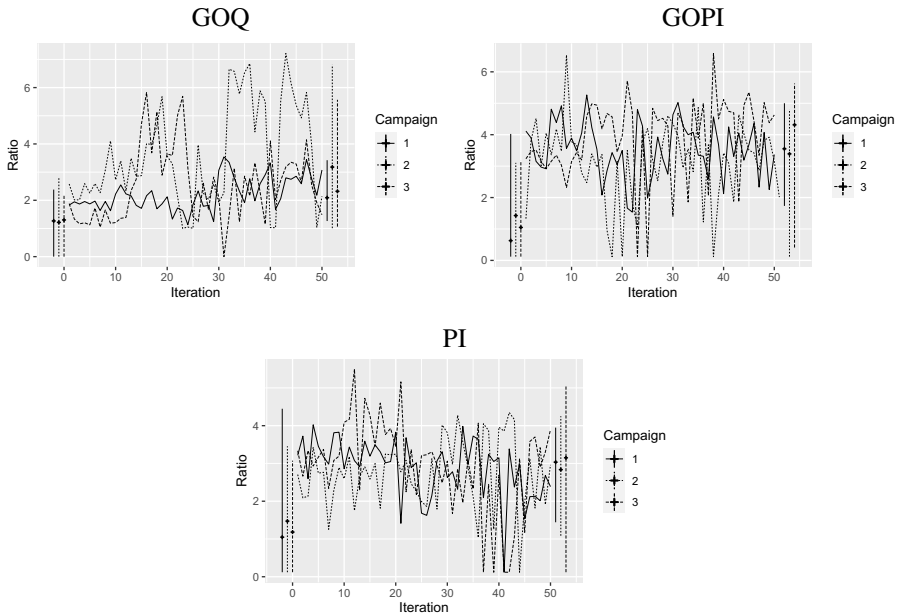


Figure 3. Quality of produced graphene (ratio of G to D intensities, higher is better) for three experimental campaigns on three different materials each. The materials shown are GOQ, GOPI, and PI. On the left of each graph (iteration ≤ 0), the distribution of ratios for the randomly-sampled parameter configurations used for the initial surrogate model for each campaign; crosses denote the median. The lines denote the progression of ratios during the iterations of the model-based optimization for the respective campaign; 50 iterations in total. The summary lines on the right of the graph (iteration > 50) show the distribution of ratios achieved during all iterations of the respective MBO run; again crosses denote the median value.

These results clearly show the promise of our approach. While MBO is given more data and better results are therefore not surprising, it performs better than random sampling in the majority of cases even when the playing field is leveled. Table 1 shows median and maximum values for 40 configurations which were randomly sampled from the total of 60 initial random samples across three experimental campaigns per material. In the column to the right of this, we show median and maximum values obtained during the first 20 iterations of the MBO that was initialized with another 20 random parameter configurations, for the same number of 40 samples seen by the optimization approach at this point. The median value achieved by the MBO is always better than for random sampling, and the best achieved ratio in seven out of nine cases. This indicates that MBO was able to optimize our target more effectively than random search. We compared our approach to configurations determined by human experts after months of investigation [20] and found similar results – the quality of graphene produced by the configurations found by MBO is up to a factor of two better than configurations found manually.

Figure 4 shows more detail for the optimization run for one of the three experimental campaigns conducted on GOQ as an example; the detailed results for the other runs are qualitatively similar. The graph illustrates how the model-based optimization proceeds and learns to optimize – the first few iterations focus on the areas of the parameter space where the initial random search has identified parameter configurations with good performance and achieves similar results. Eventually, parameter configurations with better

Mat.	Camp.	Median Value				Best Value			
		Random	40 Random	MBO first 20	all MBO	Random	40 Random	MBO first 20	all MBO
GOQ	1	1.27	1.23	1.95	2.09	2.57	2.87	2.55	3.54
GOQ	2	1.22	1.23	2.86	3.18	2.87	2.87	5.68	7.21
GOQ	3	1.3	1.23	1.69	2.32	2.39	2.87	5.83	5.83
GOPI	1	0.63	1.2	3.55	3.55	4.49	4.49	5.27	5.27
GOPI	2	1.43	1.2	3.37	3.39	3.37	4.49	6.54	6.54
GOPI	3	1.05	1.2	3.44	4.31	3.88	4.49	4.98	6.58
PI	1	1.05	1.06	3.26	3.03	5.2	3.61	4.02	4.02
PI	2	1.47	1.06	2.72	2.84	3.54	3.61	3.42	4.35
PI	3	1.18	1.06	3.41	3.15	3.13	3.61	5.5	5.5

Table 1. Median and maximum achieved G/D ratios for the initial 20 random parameter configurations, 40 random parameter configurations sampled from the total of 60 initial random samples per material, during the first 20 iterations of the MBO, and during all iterations of the MBO for all experimental campaigns. All values rounded to two decimal places.

performance are discovered and the MBO starts to focus on these areas of the parameter space, but without neglecting to explore parameter configurations that turn out to have poor performance.

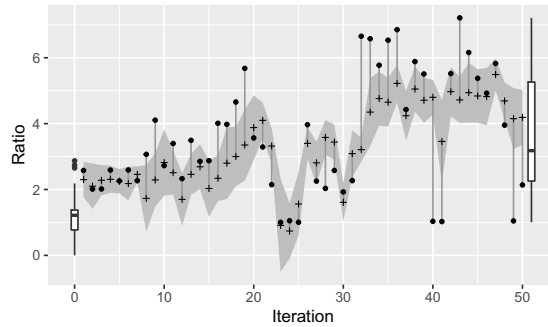


Figure 4. Quality of produced graphene (ratio of G to D intensities, higher is better) for one of the experimental campaigns on graphene oxide on quartz (GOQ). On the left of each graph, the distribution of ratios for the training data is shown (iteration 0). The circles show ground-truth data, crosses values predicted by the surrogate model (connected to the corresponding ground-truth value with a gray line). The boxplot on the right of the graph shows the distribution of ground-truth ratios of the configurations that the MBO explored.

To evaluate what the surrogate models have learned, we trained a surrogate model on the entire available data for each material; 210 evaluations from 60 random samples and 150 iterations of MBO. As the four-dimensional parameter space is not easily comprehensible, we used the mlr package [17] to compute the partial dependence of the G/D ratio on individual and pairs of parameters [21]. Figure 5 shows the corresponding plots for all pairs of continuous parameters for GOQ. They indicate that the ideal parameter configuration has low values for pressure (less than ≈ 200 psi) and time (less than ≈ 8 s), while the applied power does not seem to make a major difference. The predicted ratios are noticeably lower (darker shade of blue) above these values for pressure and time; there is no similar threshold for power.

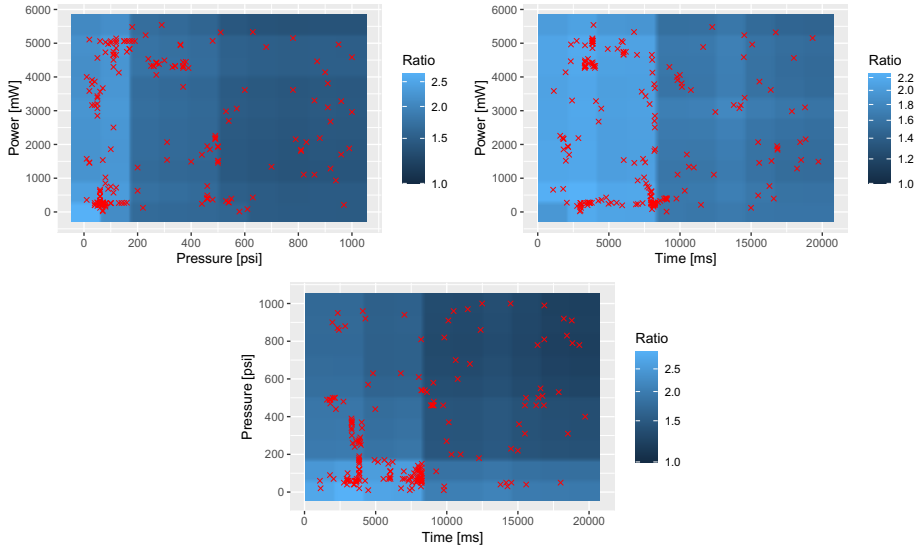


Figure 5. Partial dependence plots for pairs of continuous parameters of the predictions of a surrogate model trained on all available data for GOQ. Red crosses denote parameter configurations that were evaluated experimentally and are concentrated in the areas with the best predicted G/D ratios.

While some of these findings make sense, others do not. We know that irradiating a particular spot for too long has a detrimental effect on the material as the laser burns through it. However, the same is true for high values of laser power, but the surrogate model did not learn this relationship at all, even though parameter configurations with high power and long duration have been evaluated. Very low power and short duration regimes will have no effect on the precursor material, as the tile with a darker shade in the bottom-left corner of the plot for power and time indicates. It is unclear why low-pressure regimes are predicted to result in good ratios. The partial dependence analysis of the G/D ratio on power for graphene oxide on polyimide (GOPI, not shown for space reasons) identified values in the range of 1.9 W to 2.5 W as optimal, which coincides with the known threshold power of 2.4 W at which the conversion from polyimide to graphene occurs. Overall, our analysis of the surrogate models failed to reveal any interesting relationships that the domain experts were not already aware of or improve our understanding of the underlying processes in other ways. In some cases, the surrogate model obviously failed to learn a known relationship. There is scope for more in-depth analysis here, which may discover knowledge of interest.

3.1. Patterning Lines and Optimizing Resistance

Figure 6 shows the measured resistances for the patterned lines. We see similar results as for the spots; the optimized results are much better than the initial random data, although progress is slower. However, the median resistance of the final MBO batch is better than the minimum resistance of the initial evaluations, again conclusively demonstrating the performance of our approach. We note that this experimental setting is much more challenging for MBO because of batched evaluations – there is no immediate feedback on

a choice of parameter configuration, and proposed configurations become increasingly speculative as more “constant liar” evaluations are added.

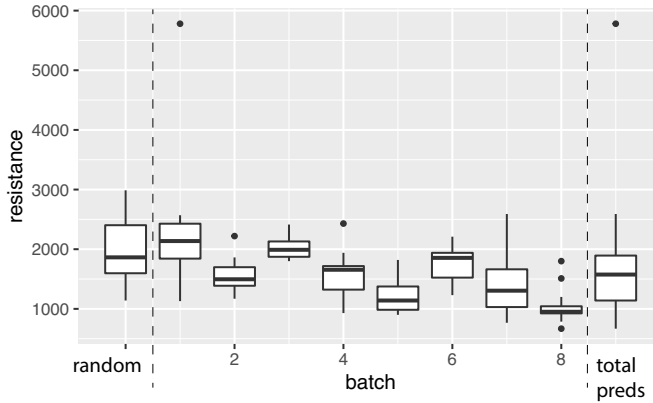


Figure 6. Quality of produced graphene (resistance in Ω) for patterning lines from graphene oxide on quartz (GOQ), lower is better. On the left of graph, the distribution of resistance for the initial training data is shown. We show results summarized by batch of 14 lines; each boxplot represents one batch. The boxplot on the right of the graph shows the distribution of measured resistances for all configurations that the MBO explored.

Similar to the experiments irradiating spots, we again analyzed what the surrogate models had learned by training a model with all evaluations and producing partial dependence plots. For space reasons, we only show the one for speed and pressure in Figure 7. Medium values for pressure and high patterning speeds result in the lowest resistance, according to the surrogate model. This intuitively makes sense, as with low speeds there is more potential for inconsistencies resulting from the irradiation. The partial dependence plots for other parameter configurations did not provide any insights, which we attribute in part to the lower total number of evaluations here than for irradiated spots.

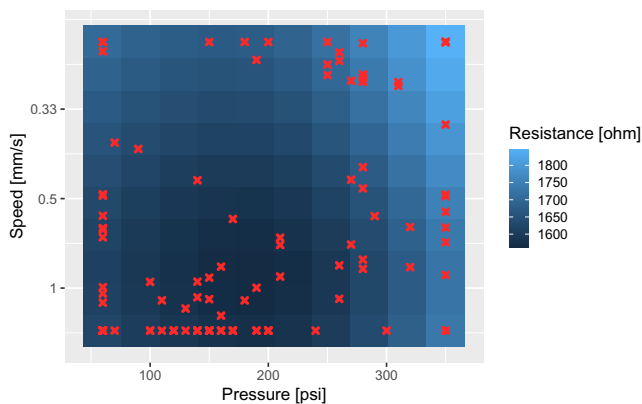


Figure 7. Partial dependence plot for patterning speed and pressure in the reaction chamber of the predictions of a surrogate model trained on all available data for patterning lines. Red crosses denote parameter configurations that were evaluated experimentally.

4. Related Work

There are numerous approaches in the literature to producing laser-induced graphene. For graphene oxide, [22] report G to D intensity ratios of up to 1.1, while [23] achieve ratios of 3.7. [24] achieve 3.45 and, with an experimental setup that is closest to ours, [25] achieve 1.03. For polyimides, [26] achieve ratios of up to 0.86, [5] 2.25, [27] 1.03, and [28] 1.38. We are not aware of any approaches that irradiate lines and measure resistance as we do here.

Most of the results in the literature are not directly comparable to ours, as the experimental setup differs. Other approaches use different kinds of lasers, pattern graphene oxide on different substrates and with different thicknesses, and use different gases in the reaction chamber. For the G/D ratios, we achieve much better results than are reported in the literature though and thus we are confident that our approach results in true improvements.

Bayesian optimization is applied in many areas of materials science. [29,30,31] use BO to optimize the grain boundary structure in polycrystalline materials instead of exhaustively evaluating the design space for the materials. They all demonstrate that results of similar quality to exhaustive evaluation can be achieved at significantly lower cost, with an increase in efficiency by up to two orders of magnitude. Similarly, [32] optimize the grain boundary energy over several thousand precomputed parameter configurations, which allows them to compare the performance of different approaches. [13] employ BO in a similar setting by evaluating its performance on a set of a few hundred precomputed results. They optimize the elastic properties of a material and demonstrate that BO is quickly able to identify the optimal parameters in their relatively small approximation of the real search space. [33] investigate the same application and in subsequent publications demonstrate the effectiveness of BO to optimize shape memory alloys [34], the band gap in perovskites, an important material in the creation of solar cells [35], and the band gap in compounds for luminescent materials [36]. [37] demonstrate the utility of BO to optimize the density-functional-theory-calculated magnetic deformation of a material, superconductors, thermoelectricity, and the strength of steel. [38] apply BO to the problem of creating new materials via a parameterized generator for patterns that describe the structure of the material. They optimize the interfacial area of the material, which can be computed directly and very cheaply compared to numerical simulations, but the large parameter space still necessitates a more efficient parameter optimization approach than exhaustive search. [39] design materials with low energy dissipation by optimizing a dopant (an impurity introduced into a pure material of a different type) and its concentration using BO.

In many applications, it may be desirable to batch evaluations of the optimized process, for example because certain measurements can only be taken after the sample has been transferred to a different instrument, as in this paper. [12] propose batches of configurations to evaluate by optimizing the acquisition functions for different values of a parameter that trades off exploration and exploitation. In contrast, we use the “constant liar” strategy [18]. [40] investigate the heat treatment of alloys, where multiple samples can be processed at the same time in an oven but at a fixed temperature, and the production of polymer fibers, where different values for polymer flow and coagulant speed can be evaluated at the same time but within a fixed geometry. They propose a nested BO

approach that optimizes the parameters that are subject to constraints in an outer loop and, given the optimized values, the unconstrained parameters in an inner loop. Their approach evaluates batches of parameter configurations where part of the parameter space is fixed. In contrast, our approach does not fix any parameter settings and does not require nested BO.

5. Conclusions and Outlook

We have applied state-of-the-art AI techniques, in particular surrogate-model-based Bayesian optimization, to the real-world problem of producing laser-induced graphene in an automated experimental setup, for both irradiating spots and lines. Patterning conductive lines into a non-conductive material will allow to produce electronic components, such as sensors. Using AI to optimize the experimental parameters, we were able to improve over results previously reported in the literature substantially. This application required no expensive customizations of existing techniques and the deployed system is used by domain experts with no background in AI.

We demonstrated the robustness of our system by optimizing for different precursor materials, different sets of initial data, different optimization objectives, and batch evaluations. Due to the cost of running experiments, we optimize with much less data than in most cases in the AI literature, but still achieve good results, in many cases after only a few iterations. This shows the usefulness this approach for small-data problems.

A promising avenue for future work is to investigate whether knowledge obtained from previous MBO runs can be used to warm-start new runs through transfer learning. In practice, no two experimental setups will be exactly the same, for example because the precursor material is manufactured in different ways, or because graphene lines instead of spots are created. It is unclear whether and how results from different experimental setups can be transferred, but this could further improve results and reduce experimental effort. Further, a principled investigation into the performance of different types of BO approaches could guide the application of MBO for materials science, in particular with respect to what machine learning techniques are most suitable for inducing surrogate models in this context.

Acknowledgments

We are supported by the University of Wyoming's College of Engineering and Applied Sciences' Engineering Initiative, the School of Energy Resources at the University of Wyoming, the Wyoming NASA Space Grant Consortium, and NASA EPSCoR. LK is supported by NSF award #1813537.

References

- [1] Ferrari AC, Bonaccorso F, Fal'ko V, Novoselov KS, Roche S, Bøggild P, et al. Science and technology roadmap for graphene, related two-dimensional crystals, and hybrid systems. *Nanoscale*. 2015;7(11):4598-810. The Royal Society of Chemistry. Available from: <http://dx.doi.org/10.1039/C4NR01600A>.
- [2] Chyan Y, Ye R, Li Y, Singh SP, Arnusch CJ, Tour JM. Laser-Induced Graphene by Multiple Lasing: Toward Electronics on Cloth, Paper, and Food. *ACS Nano*. 2018;12(3):2176-83.

- [3] Luo S, Hoang PT, Liu T. Direct laser writing for creating porous graphitic structures and their use for flexible and highly sensitive sensor and sensor arrays. *Carbon*. 2016;96:522-31. Available from: <http://www.sciencedirect.com/science/article/pii/S0008622315302943>.
- [4] Ye R, Peng Z, Wang T, Xu Y, Zhang J, Li Y, et al. In Situ Formation of Metal Oxide Nanocrystals Embedded in Laser-Induced Graphene. *ACS Nano*. 2015 Sep;9(9):9244-51. Publisher: American Chemical Society. Available from: <https://doi.org/10.1021/acsnano.5b04138>.
- [5] Lin J, Peng Z, Liu Y, Ruiz-Zepeda F, Ye R, Samuel ELG, et al. Laser-induced porous graphene films from commercial polymers. *Nature Communications*. 2014 Dec;5(1):5714. Available from: <https://doi.org/10.1038/ncomms6714>.
- [6] El-Kady MF, Kaner RB. Scalable fabrication of high-power graphene micro-supercapacitors for flexible and on-chip energy storage. *Nature Communications*. 2013 Feb;4:1475. Available from: <https://doi.org/10.1038/ncomms2446>.
- [7] Sygletou M, Tzourmpakis P, Petridis C, Konios D, Fotakis C, Kymakis E, et al. Laser induced nucleation of plasmonic nanoparticles on two-dimensional nanosheets for organic photovoltaics. *J Mater Chem A*. 2016;4(3):1020-7. Available from: <http://dx.doi.org/10.1039/C5TA09199C>.
- [8] Wang F, Wang K, Zheng B, Dong X, Mei X, Lv J, et al. Laser-induced graphene: preparation, functionalization and applications. *Materials Technology*. 2018;33(5):340-56. Available from: <https://doi.org/10.1080/10667857.2018.1447265>.
- [9] Wan Z, Streed EW, Lobino M, Wang S, Sang RT, Cole IS, et al. Laser-Reduced Graphene: Synthesis, Properties, and Applications. *Advanced Materials Technologies*. 2018;3(4):1700315.
- [10] Wan Z, Wang S, Haylock B, Kaur J, Tanner P, Thiel D, et al. Tuning the sub-processes in laser reduction of graphene oxide by adjusting the power and scanning speed of laser. *Carbon*. 2019;141:83-91. Available from: <http://www.sciencedirect.com/science/article/pii/S0008622318308443>.
- [11] Wahab H, Jain V, Tyrrell AS, Seas MA, Kotthoff L, Johnson PA. Machine-learning-assisted fabrication: Bayesian optimization of laser-induced graphene patterning using in-situ Raman analysis. *Carbon*. 2020;167:609-19. Available from: <http://www.sciencedirect.com/science/article/pii/S0008622320305285>.
- [12] Häse F, Roch LM, Kreisbeck C, Aspuru-Guzik A. Phoenix: A Bayesian Optimizer for Chemistry. *ACS Central Science*. 2018 Sep;4(9):1134-45. Available from: <https://doi.org/10.1021/acscentsci.8b00307>.
- [13] Talapatra A, Boluki S, Duong T, Qian X, Dougherty E, Arróyave R. Autonomous efficient experiment design for materials discovery with Bayesian model averaging. *Phys Rev Materials*. 2018 Nov;2(11):113803. Available from: <https://link.aps.org/doi/10.1103/PhysRevMaterials.2.113803>.
- [14] Marciano D, Kosynkin D, Berlin J, Sinitiskii A, Sun Z, Slesarev A, et al. Improved synthesis of graphene oxide. *ACS Nano*. 2010 Aug;4(8):4806-14.
- [15] Jones DR, Schonlau M, Welch WJ. Efficient Global Optimization of Expensive Black-Box Functions. *J of Global Optimization*. 1998 Dec;13(4):455-92. Available from: <http://dx.doi.org/10.1023/A:1008306431147>.
- [16] Bischl B, Richter J, Bossek J, Horn D, Thomas J, Lang M. mlrMBO: A Modular Framework for Model-Based Optimization of Expensive Black-Box Functions. *arXiv:170303373*. 2017. Available from: <http://arxiv.org/abs/1703.03373>.
- [17] Bischl B, Lang M, Kotthoff L, Schiffner J, Richter J, Studerus E, et al. mlr: Machine Learning in R. *Journal of Machine Learning Research*. 2016;17(170):1-5. Bibtext: *JMLR:v17:15-066*. Available from: <http://jmlr.org/papers/v17/15-066.html>.
- [18] Ginsbourger D, Le Riche R, Carraro L. Kriging Is Well-Suited to Parallelize Optimization. In: Tenne Y, Goh CK, editors. *Computational Intelligence in Expensive Optimization Problems*. Berlin, Heidelberg: Springer Berlin Heidelberg; 2010. p. 131-62. Available from: https://doi.org/10.1007/978-3-642-10701-6_6.
- [19] Beckham JL, Wyss KM, Xie Y, McHugh EA, Li JT, Advincula PA, et al. Machine Learning Guided Synthesis of Flash Graphene. *Advanced Materials*. 2022;34(12):2106506. eprint: <https://onlinelibrary.wiley.com/doi/pdf/10.1002/adma.202106506>. Available from: <https://onlinelibrary.wiley.com/doi/abs/10.1002/adma.202106506>.
- [20] Kotthoff L, Jain V, Tyrrell A, Wahab H, Johnson P. AI for Materials Science: Tuning Laser-Induced Graphene Production. In: *Data Science Meets Optimisation Workshop at IJCAI 2019*; 2019. .
- [21] Goldstein A, Kapelner A, Bleich J, Pitkin E. Peeking Inside the Black Box: Visualizing Statistical

- Learning With Plots of Individual Conditional Expectation. *Journal of Computational and Graphical Statistics*. 2015;24(1):44-65.
- [22] Zhang Y, Guo L, Wei S, He Y, Xia H, Chen Q, et al. Direct imprinting of microcircuits on graphene oxides film by femtosecond laser reduction. *Nano Today*. 2010;5(1):15-20. Available from: <http://www.sciencedirect.com/science/article/pii/S1748013210000046>.
- [23] Guan YC, Fang YW, Lim GC, Zheng HY, Hong MH. Fabrication of Laser-reduced Graphene Oxide in Liquid Nitrogen Environment. *Scientific Reports*. 2016 Jun;6:28913. Available from: <https://doi.org/10.1038/srep28913>.
- [24] Sokolov DA, Rouleau CM, Geohegan DB, Orlando TM. Excimer laser reduction and patterning of graphite oxide. *Carbon*. 2013;53:81-9. Available from: <http://www.sciencedirect.com/science/article/pii/S0008622312008470>.
- [25] Tao Y, Varghese B, Jaiswal M, Wang S, Zhang Z, Oezylmaz B, et al. Localized insulator-conductor transformation of graphene oxide thin films via focused laser beam irradiation. *Applied Physics A*. 2012 Mar;106(3):523-31. Available from: <https://doi.org/10.1007/s00339-011-6710-8>.
- [26] In JB, Hsia B, Yoo JH, Hyun S, Carraro C, Maboudian R, et al. Facile fabrication of flexible all solid-state micro-supercapacitor by direct laser writing of porous carbon in polyimide. *Carbon*. 2015;83:144-51. Available from: <http://www.sciencedirect.com/science/article/pii/S0008622314010896>.
- [27] Luong DX, Subramanian AK, Silva GAL, Yoon J, Cofer S, Yang K, et al. Laminated Object Manufacturing of 3D-Printed Laser-Induced Graphene Foams. *Advanced Materials*. 2018;30(28):1707416. Available from: <https://onlinelibrary.wiley.com/doi/abs/10.1002/adma.201707416>.
- [28] Hawes GF, Yilman D, Noremberg BS, Pope MA. Supercapacitors Fabricated via Laser-Induced Carbonization of Biomass-Derived Poly(furfuryl alcohol)/Graphene Oxide Composites. *ACS Applied Nano Materials*. 2019;2:6312-24.
- [29] Kiyohara S, Oda H, Tsuda K, Mizoguchi T. Acceleration of stable interface structure searching using a kriging approach. *Japanese Journal of Applied Physics*. 2016 Mar;55(4):045502.
- [30] Kikuchi S, Oda H, Kiyohara S, Mizoguchi T. Bayesian optimization for efficient determination of metal oxide grain boundary structures. *Physica B: Condensed Matter*. 2018;532:24-8. Special issue on Frontiers in Materials Science: Condensed Matters.
- [31] Bondevik T, Kuwabara A, Løvrvik OM. Application of machine learning-based selective sampling to determine BaZrO₃ grain boundary structures. *Computational Materials Science*. 2019;164:57-65.
- [32] Ueno T, Rhone TD, Hou Z, Mizoguchi T, Tsuda K. COMBO: An efficient Bayesian optimization library for materials science. *Materials Discovery*. 2016;4:18-21.
- [33] Balachandran PV, Xue D, Theiler J, Hogden J, Lookman T. Adaptive Strategies for Materials Design using Uncertainties. *Scientific Reports*. 2016 Jan;6:19660. Available from: <https://doi.org/10.1038/srep19660>.
- [34] Xue D, Balachandran PV, Hogden J, Theiler J, Xue D, Lookman T. Accelerated search for materials with targeted properties by adaptive design. *Nature Communications*. 2016 Apr;7:11241. Available from: <https://doi.org/10.1038/ncomms11241>.
- [35] Paliana G, Gubernatis JE, Lookman T. Multi-fidelity machine learning models for accurate bandgap predictions of solids. *Computational Materials Science*. 2017;129:156-63.
- [36] Lookman T, Balachandran PV, Xue D, Yuan R. Active learning in materials science with emphasis on adaptive sampling using uncertainties for targeted design. *npj Computational Materials*. 2019 Feb;5(1):21.
- [37] Ling J, Hutchinson M, Antono E, Paradiso S, Meredig B. High-Dimensional Materials and Process Optimization Using Data-Driven Experimental Design with Well-Calibrated Uncertainty Estimates. *Integrating Materials and Manufacturing Innovation*. 2017 Sep;6(3):207-17.
- [38] Hankins S, Kothhoff L, Fertig RS. Bio-like Composite Microstructure Designs for Enhanced Damage Tolerance via Machine Learning. In: *American Society for Composites 34th Annual Technical Conference*; 2019. .
- [39] Dehghannasiri R, Xue D, Balachandran PV, Yousefi MR, Dalton LA, Lookman T, et al. Optimal experimental design for materials discovery. *Computational Materials Science*. 2017;129:311-22.
- [40] Vellanki P, Rana S, Gupta S, Rubin D, Sutti A, Dorin T, et al. Process-constrained batch Bayesian optimisation. In: *Guyon I, Luxburg UV, Bengio S, Wallach H, Fergus R, Vishwanathan S, et al., editors. Advances in Neural Information Processing Systems*. Curran Associates, Inc.; 2017. p. 3414-23.